

Ultra-Relativistic Magneto-Hydro-Dynamic Jets in the context of Gamma Ray Bursts

Christian Fendt¹

*Institut für Physik, Universität Potsdam, Am Neuen Palais 10, D-14469 Potsdam,
Germany*

cfendt@aip.de

and

Rachid Ouyed

*Department of Physics and Astronomy, University of Calgary, 2500 University Drive NW,
Calgary, Alberta, T2N 1N4 Canada*

ouyed@phas.ucalgary.ca

ABSTRACT

We present a detailed numerical study of the dynamics and evolution of ultrarelativistic magnetohydrodynamic jets in the black hole-disk system under extreme magnetization conditions. We find that Lorentz factors of up to 3000 are achieved and derived a modified Michel scaling ($\Gamma \sim \sigma$) which allows for a wide variation in the flow Lorentz factor. Pending contamination induced by mass-entrainment, the linear Michel scaling links modulations in the ultrarelativistic wind to variations in mass accretion in the disk for a given magnetization. The jet is asymptotically dominated by the toroidal magnetic field allowing for efficient collimation. We discuss our solutions (jets) in the context of Gamma ray bursts and describe the relevant features such as the high variability in the Lorentz factor and how high collimation angles ($\sim 0^\circ - 5^\circ$), or cylindrical jets, can be achieved. We isolate a jet instability mechanism we refer to as the “bottle-neck” instability which essentially relies on a high magnetization and a recollimation of the magnetic flux surfaces. The instability occurs at large radii where any dissipation of the magnetic energy into radiation would in principle result in an optically thin emission.

Subject headings: gamma rays:bursts — magnetic fields — MHD — ISM:jets and outflows

¹Also: Astrophysikalisches Institut Potsdam, An der Sternwarte 16, D-14482 Potsdam, Germany

1. Introduction

It is widely accepted that the most conventional interpretation of the observed GRBs result from the conversion of the kinetic energy of ultra-relativistic particles (wind) to radiation in an optically thin region. The particles being accelerated by a fireball mechanism taking place near the central engine (Goodman 1986; Shemi & Piran 1990; Paczyński 1990). The prompt γ -ray emission is probably induced by internal shocks within the wind while the afterglow results from the wind external shock interacting with the surrounding medium. The Lorentz factor Γ of the relativistic wind must reach high values ($\Gamma \sim 10^2 - 10^3$) both to produce γ -rays and to avoid photon-photon annihilation along the line of sight, whose signature is not observed in the spectra of GRBs (Goodman 1986). The crucial point is that for a range of plausible parameters, the prompt occurs above the Compton photosphere (Mészáros 2002).

Whether produced locally or originating from the source, large magnetic fields are required to account for the synchrotron and/or inverse Compton emission from a non-thermal population of accelerated electrons produced behind the (internal and external) shock waves. In the case of the afterglow emission, the magnetic field has to be locally generated by microscopic processes (Meszaros & Rees 1993; Wijers, Rees, & Meszaros 1997; Thompson & Madau 2000). In the case of the prompt γ -ray emission, such a locally generated magnetic field is also usually invoked (Rees & Meszaros (1994); Papatianassiou & Meszaros (1996); Sari & Piran (1997)). Although a large scale field originating from the hidden source could play the same role (Meszaros & Rees 1993, 1997; Tavani 1996).

Support for a high collimation of these winds is derived from the break in the light curves of afterglows for long duration gamma ray bursts (e.g. Stanek et al. (1999)). The brightness of the optical transient associated to GRB990123 showed a break (Kulkarni et al. 1999), and a steepening from a power law in time proportional to $t^{-1.2}$, ultimately approaching a slope $t^{-2.5}$ (Castro-Tirado et al. 1999). The achromatic steepening of the optical light curve and early radio flux decay of GRB 990510 are inconsistent with simple spherical expansion, and well fit by jet evolution.

The high Lorentz factors invoked, the reference to a magnetic field and the high collimation are ingredients suggestive of magnetized jets at play in these phenomena. The extreme magnetic fields led to models using a highly magnetized millisecond pulsar. However, due to the baryon loading, GRB jets are different from the essentially baryon-free pulsar wind case (e.g. Usov (1994)). Magnetohydrodynamic (MHD) jets emanating from the surface of an accretion disk surrounding a central object are naturally loaded with baryons and offer a more interesting case for GRBs. Necessary currents are maintained given the standard baryon/mass loading which guarantees the validity of the MHD approximation out to large

distances (up to 10^{20} cm; Spruit et al. (2001) and Appendix A in this paper). The MHD approximation simplifies the mathematical treatment of the problem but on the other hand internal magnetic energy dissipation mechanisms are to be sought that would lead to the proper (GRB-like) emission. The MHD approximation breaks down when the flow reaches the critical radius beyond which current can no longer be sustained; we will refer to this radius as the *MHD radius*. Note that for the pulsar wind case, the MHD approximation breaks down much earlier, and plasma theories of large amplitude electromagnetic waves are applied to explain the prompt emission (Lyutikov & Blackman 2001). Here, we focus on MHD jets emanating from the disk-black hole system (Thompson 1994; Meszaros & Rees 1997). We are interested in solutions that account for the crucial features inherent to GRB models such as i) the extreme and variable Lorentz factors as in the internal shock model, ii) the high collimation ($\theta \sim 1^\circ - 10^\circ$), iii) the dissipation mechanisms. We start in Sec. 2 by introducing the reader to the basic concepts of MHD jets before specifically focusing on the acceleration (Sec. 3) and collimation (Sec. 4) mechanisms. In Sec. 5, we apply our results to GRBs and discuss ultra-relativistic jets within the standard internal-external shock model of GRBs. In Sec. 6, we isolate a mechanism for jet instability occurring at large radii (beyond the photosphere) for the case of extreme Lorentz factor and associate it with possible dissipation mechanisms. We summarize our results in Sec. 7.

2. Basic concepts of relativistic MHD jets

2.1. Magnetohydrodynamic jets

The scenario of MHD jet formation (Blandford & Payne 1982; Pudritz & Norman 1983; Camenzind 1986) can be summarized as follows. The jet is initiated as a slow wind from the inner disk by a process which is not yet completely understood, in particular its time-dependent character. Most probably, some disk instability is responsible for ejecting the matter in the direction perpendicular to the disk surface. The disk wind is first launched magneto-centrifugally and further accelerated and (self-) collimated into a narrow beam by Lorentz forces.

Two key parameters which determine the dynamics of relativistic MHD jet flows, (i) the plasma magnetization σ and (ii) the light cylinder of the magnetosphere R_L . These will be discussed below.

Considerations of stationary MHD flows have revealed that relativistic jets must be strongly magnetized (Michel 1969; Camenzind 1986; Li et al. 1992; Fendt & Camenzind 1996). In that case, the available magnetic energy can be transferred over a small amount

of mass with high kinetic energy. On the other hand, a very strong magnetization may be in conflict with the MHD assumption lacking a sufficient large amount of electric charges which are needed to drive the electric current system (see §3.6).

Theoretical modelling of jet formation requires to solve the governing MHD equations. However, due to the complexity of MHD and the astrophysical boundary conditions indicated, a completely self-consistent MHD solution for the jet formation process being compatible with all the generic features (MHD self-collimation, accretion-ejection mechanism, magnetic field generation, spatial and time scales etc.) does not yet exist.

In this paper, we will concentrate on solutions to the *stationary, axisymmetric, ideal MHD* equations in the relativistic limit. Then the jet magnetic field distribution can be described by a bunch of nested axisymmetric surfaces, measuring the magnetic flux through a circular area around the symmetry axis. $\Psi = (1/2\pi) \int \vec{B}_P \cdot d\vec{A}$. The stationary approach has the advantage to obtain a *global* solution for the relativistic jet MHD structure (e.g. Li (1993); Fendt (1997)) on spatial scales and with a resolution which cannot (yet) be reached by time-dependent simulations (Kudoh et al. 1998; Koide et al. 2000). Long-term (Newtonian) MHD simulations, however, possess the ability to demonstrate the self-collimation of MHD jets (Ouyed & Pudritz 1997; Ouyed et al. 2003).

2.2. The magnetization parameter

The essential parameter for MHD jets is the *magnetization* parameter (Michel 1969),

$$\sigma = \frac{\Phi^2 \Omega_F^2}{4\dot{M}c^3}. \quad (1)$$

The iso-rotation parameter $\Omega_F(\Psi)$ is frequently interpreted as the angular velocity of the magnetic field lines. The function $\Phi = B_p r^2$ is a measure of the magnetic field distribution (see Li (1993)), and $\dot{M} \equiv \pi \rho v_p R^2$ is the mass flow rate within the flux surface. Equation (1) demonstrates that the launch of a highly relativistic (i.e. highly magnetized) jet essentially requires at least one of three conditions – a rapid rotation, a strong magnetic field and/or a comparatively low mass load.

In the case of a spherical outflow ($\Phi = const$) with negligible gas pressure one may derive the Michel scaling between the asymptotic Lorentz factor and the flow magnetization,

$$\Gamma_\infty = \sigma^{1/3} \quad (2)$$

(Michel 1969). Assuming a constant mass flux across a jet with magnetic flux Φ_{jet} and mass flow rate \dot{M}_{jet} , the Michel scaling gives $\Gamma_\infty = (\Omega_F \Phi)^{2/3} (\dot{M}_{jet})^{-1/3}$. It must be mentioned

already that Eq. (2) relies on further constraints. For a general relation $\Gamma_\infty(\sigma)$ the influence of collimation, gravity and gas pressure² must be considered.

Depending on the exact magnetic field distribution $\Phi(r, z)$, in a *collimating jet* the matter can be substantially accelerated beyond the fast point magnetosonic point (Begelman & Li 1994; Fendt & Camenzind 1996), as it is moved from infinity to a finite radius of several Alfvén radii. As a result, the power law index in Eq. (2) can be different from the Michel-scaling (see Sec. 3.5; Fendt & Camenzind (1996); Vlahakis & Königl (2001)). If the $\Phi(r; \Psi)$ is decreasing outwards, the asymptotic flow is dominated by the kinetic energy (Begelman & Li 1994). Still, the speed of the flow at the fast point follows the Michel scaling Eq. (2), $\Gamma_{\text{FM}} = \sigma(\Psi)^{1/3}$.

The function $\Phi(r; z(\Psi)) = \Phi(r; \Psi)$ describes the *opening* of the magnetic flux surfaces $\Psi(r, z)$ comparable to the action of a “magnetic nozzle” (Camenzind 1989; Li et al. 1992). A flux function Φ constant along the field lines as applied in the Michel scaling corresponds to a constant opening angle of the magnetic field.

2.3. Relativistic features

At the *light cylinder* (hereafter l.c.) the velocity of the magnetic field lines “rotating” with angular velocity $\Omega_{\text{F}}(\Psi)$ coincides with the speed of light. The l.c. is located at the cylindrical radius

$$R_{\text{L}}(\Psi) = c/\Omega_{\text{F}}(\Psi). \quad (3)$$

For a differential rotation of the field line foot points as in an accretion disk,

the cylinder deforms into a *light surface* (of a priori unknown shape)³. The l.c. has to be interpreted as the Alfvén surface in the limit of vanishing matter density (force-free limit). Outside the l.c. the magnetic field lines “rotate” faster than the speed of light⁴. The existence of a strong toroidal field component allows the matter, being frozen into the field, to *slide along* the field which guarantees $v < c$ also in the region $R > R_{\text{L}}$.

The location of the l.c. determines the relativistic character of the magnetosphere. If the light cylinder is comparable to the dimensions of the object investigated, a relativistic

²In the case of a “hot wind”, the magnetization is not a free parameter anymore.

³Note that general relativistic effects affect the shape of the light cylinder. Frame dragging close to a rotating black hole implies a second light surface.

⁴As the field line is not a physical object, the laws of physics are not violated.

treatment of MHD is required.

Contrary to Newtonian MHD, in the relativistic case *electric fields* cannot be neglected. The poloidal electric field component is directed perpendicular to the magnetic flux surface. Its strength scales with the l.c. radius, $E_p = E_\perp = (r/R_L)B_p$. As a consequence of $E_p \simeq B_p$, the effective magnetic pressure can be lowered by a substantial amount (Begelman & Li Begelman & Li (1994)).

A further difference between relativistic and Newtonian MHD is the fact that the poloidal Alfvén speed u_A becomes complex for $r > R_L$, $u_A^2 \sim B_p^2 (1 - (r/R_L)^2) = B_p^2 - E_\perp^2$. Therefore, Alfvén waves cannot propagate beyond the l.c. and only fast magnetosonic waves are able to exchange information across the jet.

Note that the l.c. arises as a relativistic effect due to the *rapid rotation* of the magnetosphere. This has to be distinguished from the *fast proper motion* of matter in poloidal direction leading to relativistic effects affecting the inertial forces. For relativistic MHD jets, both features are interrelated. A rapidly propagating jet must originate in a rapidly rotating source. This interrelation is parameterized by the Michel-scaling.

The l.c. is essentially a *special relativistic* feature. Close to the black hole horizon *general relativity* becomes relevant. The existence of the l.c. as a natural length scale in relativistic MHD is not consistent with the assumption of a *self-similar* jet structure. The latter holds even more when general relativistic effects are considered (see Sec. 4).

2.4. Magnetization of GRB jets

In this paper we discuss the possibility that GRBs are generated by ultra-relativistic MHD jets. Essentially, two model scenarios for the jet origin may be considered, a jet launched from an accretion disk or by a highly magnetized neutron star. As the properties of the central source driving the jet are yet unknown, any estimate on the jet magnetization – magnetic field distribution, mass flow rate and rotation – must rely on somewhat hypothetical parameters. In the following, we will assume that the jet is launched from the accretion disk around a collapsed object and estimate the jet magnetization by constraints from disk theory. We do not consider the origin of the disk magnetic field. It could be advected within the disk from the ambient medium, or generated by a disk dynamo.

We constrain the jet magnetization at the foot point radius r_\star of the jet $\sigma = (B_{p\star}^2 r_\star^4 \Omega_F^2 / c^3 \dot{M}_{\text{jet}})$, from the disk equipartition field strength $B_{\text{eq}}^2 \simeq P_{\text{gas}}$. This value limits the toroidal magnetic field component which can be built up by the disk differential rotation, $B_T \lesssim B_{\text{eq}}$ and also

for the poloidal magnetic field amplification by a dynamo process, $B_P \lesssim B_T$. In the case of a self-similar advection dominated disk with accretion rate \dot{M}_{acc} , we obtain

$$B_{\text{eq}} \simeq 7.8 \times 10^9 \text{ G} \left(\frac{\alpha}{10^{-2}} \right)^{-1/2} \left(\frac{M}{M_\odot} \right)^{-1/2} \left(\frac{\dot{M}_{\text{acc}}}{\dot{M}_E} \right)^{1/2} \left(\frac{r}{r_S} \right)^{-5/4}, \quad (4)$$

where $\dot{M}_E = 10 L_\odot / c^2 = 2.2 \times 10^{-8} (M/M_\odot) M_\odot \text{yr}^{-1}$ is the Eddington accretion rate, α is the disk viscosity parameter, and r_S the Schwarzschild radius (Narayan et al. (1998), see also Fendt & Greiner (2001)). An optically thin standard accretion disk with Thomson opacity gives a similar value. A number of GRB jet models discussed in the literature consider magnetic field strengths of up to 10^{15}G (e.g. Lyutikov & Blackman (2001)). Equation (4) shows that such a high field strength can never be expected from a disk magnetic field for sub-Eddington accretion rates. Hyper-accreting disks around black holes have been discussed by Popham et al. (1999). These models provide accretion rates of 0.01 to $10 M_\odot \text{s}^{-1}$ and consider efficient cooling by neutrino losses. As a consequence, the equipartition field strength may reach $10^{14} - 10^{15} \text{G}$. We note however that α is unknown for hyper-accreting disks.

The other parameter in the magnetization is the jet mass flow rate. As this is unknown, we scale the jet mass flow rate in terms of the disk accretion rate, $\dot{M}_{\text{jet}} \simeq 10^{-3} \dot{M}_{\text{acc}}$. An upper limit for the jet magnetization can be derived considering the marginally stable orbit as jet origin, $r_\star = r_{\text{ms}}$. Here, we find the largest disk magnetic field strength, together with the most rapid rotation, $\Omega_F \simeq 1.4 \times 10^4 (M/M_\odot)^{-1} (r_\star/3r_S)^{-3/2}$ (in the Schwarzschild case). For a maximally rotating black hole, $(a/M) \simeq 1$, we have $r_{\text{ms}} \simeq r_g$, where r_g is the gravitational radius of the black hole. With the maximum jet magnetic flux constrained by the disk equipartition field, $B_\star \simeq B_{\text{eq}}$, the jet magnetization essentially depends on two parameters – the mass ejection rate and the jet origin,

$$\sigma \simeq 10^5 \left(\frac{\alpha}{10^{-2}} \right)^{-1} \left(\frac{\dot{M}_{\text{jet}}}{10^{-3} \dot{M}_{\text{acc}}} \right)^{-1} \left(\frac{r_\star}{3r_g} \right)^{-3/2}. \quad (5)$$

From the Michel-scaling, Eq. (2), we derive a minimum asymptotic jet Lorentz factor $\Gamma_\infty \simeq 10$.

GRB afterglow observations indicate a total baryonic mass in the burst of about $10^{-6} M_\odot$ (Piran 1999), implying a hypothetical jet mass flow rate of about $\dot{M}_{\text{jet}} \simeq 10^{-7} M_\odot \text{s}^{-1}$ if the burst lasts for 10 s. Such mass flow rates can never be achieved for disk accretion rates constrained by the Eddington limit,

$$\dot{M}_{\text{jet}} \simeq 1.4 \times 10^{-17} M_\odot \text{s}^{-1} \left(\frac{\alpha}{10^{-2}} \right)^{-1} \left(\frac{M}{M_\odot} \right) \quad (6)$$

$$\cdot \left(\frac{\dot{M}_{\text{acc}}}{\dot{M}_{\text{E}}} \right) \left(\frac{r_{\star}}{r_{\text{S}}} \right)^{-3/2} \left(\frac{\sigma}{1000} \right)^{-1}.$$

The hyper-accreting stages of accretion disks discussed by Popham et al. (1999) are a way out of this dilemma. With $\dot{M}_{\text{jet}} \simeq 10^{-3} \dot{M}_{\text{acc}}$, the inferred accretion rate could be $\lesssim 10^{-2} M_{\odot} \text{ s}^{-1}$ (necessary for neutrino cooling) and the equipartition field strength is increased substantially. However, the flow magnetization governing the asymptotic speed will remain about the same.

3. Acceleration – the asymptotic Lorentz factor

Assuming axisymmetry and stationarity, the equations of ideal MHD can be re-written into two equations describing the force-balance along the field (the *MHD wind equation*, hereafter WE) and the force-balance across the field (the *Grad-Shafranov equation*, hereafter GSE). In general, both equations are interrelated as the source term of the GSE depends on the dynamics of the MHD wind solution. In turn, the wind acceleration depends on the magnetic field structure which is given by the solution of the GSE. However, in the case of highly relativistic (i.e. highly magnetized) jets, the influence of the moving matter on the magnetic field can be neglected and the field structure may be calculated by the *force-free* GSE (see Sec. 4).

In this section we present ultra-relativistic MHD solutions of the wind equation. For simplicity, we will consider the *cold* wind equation in Minkowski space-time, which gives us the freedom to investigate the flow dynamics for a different choice of magnetization. For a hot wind MHD solution in Kerr metric we refer to Fendt & Greiner (2001).

As the kinetic time scale for the GRB jet propagation, τ_{kin} , is well above the time scale when the jet crosses the collimation region, τ_{coll} ,

$$\tau_{\text{coll}} \simeq \frac{10R_{\text{L}}}{c} \simeq 3 \times 10^{-3} \text{ s} \ll \tau_{\text{kin}} = \frac{10^{12} \text{ cm}}{c} \simeq 33 \text{ s} \quad (7)$$

stationarity may indeed be applied for the jet formation region.

3.1. The relativistic MHD wind equation

Combining the MHD equation of motion with the conservation laws for energy E , angular momentum L , magnetization σ and iso-rotation Ω_{F} , we obtain the *wind equation* for the poloidal velocity $u_{\text{p}} = \Gamma v_{\text{p}}/c$ in Minkowski space-time,

$$u_{\text{p}}^2 + 1 = \quad (8)$$

$$E^2 \frac{x^2(1 - M^2 - x_A^2)^2 - (x^2(1 - x_A^2) - x_A^2 M^2)^2}{x^2(1 - M^2 - x^2)^2},$$

(Camenzind 1986). Here, $x_A^2 = (\Omega_F L/E)$ defines the Alfvén radius x_A and $M_A^2 = (4\pi\mu n' u_p^2)/B_p^2$ the Alfvén Mach number M_A (n' is the proper particle density). In the cold wind limit the wind equation simplifies to a polynomial equation of degree of four for the poloidal velocity. The polynomial coefficients explicitly depend on the magnetization σ , the flux tube function Φ , and the flow parameters energy E and angular momentum L (see Fendt & Camenzind (1996); Fendt & Greiner (2001)).

At the magnetosonic points the wind equation becomes singular. A finite solution only exists if numerator and denominator vanishes together. For this *critical* wind solution the poloidal velocity of the matter equals the speed of the magnetosonic waves at the magnetosonic points. We consider such a solution as a *global* solution as it is accelerating from low velocities at small radii to large speed at large radii.

The cold wind solution is defined by the following parameter set. The magnetization σ and the iso-rotation Ω_F are free parameters and may be constraint by the astrophysical boundary conditions. The total energy density of the flow E is constrained by the regularity condition at the fast point. With Ω_F and E also the total angular momentum flow $L = E/\Omega_F$ is determined.

3.2. The ultra-relativistic asymptotic MHD jet

Figure 1 shows a sample of MHD jet solutions for a parameter set as motivated above⁵. We have calculated the flow dynamics for different magnetization $\sigma = 1000$ and $\sigma = 5000$, and for a different magnetic field distribution $\Phi(r; \Psi) \sim r^{-q}$ with $q = 0.01, 0.1, 0.2$. The light cylinder is located at $R_L = 10^7 \text{cm}$. Gravity is unimportant in the cold limit. Thus, the degree of collimation does not change the character of the solution as a function of radius r (e.g. $u_p(r)$). However, for a collimated flow, for each radius r the distance from the source $z(r)$ is increasing with increasing degree of collimation.

Our solutions demonstrate that ultra-relativistic velocities can be achieved by a MHD

⁵The figure shows the two positive solution branches out of the set of four numerical solutions of the wind equation at each radial point. The branch which starts with low velocity at small radius and accelerates to high speed at large radii is the continuous branch of the (stationary) *physical wind solution*. The other one decelerates with radius and is not defined for each radius. For an appropriate parameter set, the latter branch may turn into a continuous *accretion branch*. The intersections of these branches identify the magnetosonic points (the Alfvén point at $R \simeq R_L$ and fast magnetosonic point at $R > R_L$) which determine the solution.

jet if it is highly magnetized. We obtain velocities up to $u_p \simeq \Gamma \simeq 3000$ for $\sigma = 5000$. From the sequence of plots in Fig.1 it can be seen that magnetization σ and field distribution (parameter q) play an equally important role concerning the jet acceleration. A similar gain in asymptotic velocity can be achieved by either increasing the magnetization by a factor of five *or* increasing q from close to the Michel value to 0.1 (compare upper right with middle left figure). This confirms earlier results by Begelman & Li (1994) and Fendt & Camenzind (1996).

3.3. Pitch angle of the magnetic field

It is well known from MHD wind theory that the motion of matter along poloidal magnetic field lines also implies induction of a strong *toroidal* field component – so strong that it overcomes the poloidal component for radii larger than the Alfvén radius. This has been shown early in the case of non-relativistic self-similar MHD disk winds (Blandford & Payne 1982), but holds also for jet flows launched from the disk around a rotating black hole (Fendt & Greiner 2001). For the MHD jet solutions presented in the present paper we find the same result (not shown). In particular, the latter paper shows a power law distribution for the toroidal magnetic field decay in radial direction for radii larger than the light cylinder, $B_T \sim r^{-1}$. The poloidal magnetic field strength, however, decays faster, as $q \lesssim 0$ for any reasonable field distribution. For a monopole type field we have $q = 0$ and $B_p \sim r^{-2}$ while for a dipolar field $B_p \sim r^{-3}$ and $q = -1$. For the solutions presented here, for the “asymptotic” domain (i.e. for $r = 10^4, z \simeq 10^7$) the numerical solution gives $B_T/B_p \simeq 10^4$.

Essentially, this proves again the well known characteristics of a magnetohydrodynamic jet which is asymptotically dominated by the toroidal magnetic field component. This may have important implications e.g. for the magnetic field distribution in the asymptotic shocks and for the interpretation of the polarization structure in the afterglow observations (see Sec. 6).

3.4. Energy balance along the flow

MHD jets essentially live from the exchange of magnetic and kinetic energy. When the jet is launched with low velocity, the energy content is mainly in the magnetic part, i.e. we have a *Poynting dominated* flow. As the flow accelerates, it gains kinetic energy converting Poynting flux into kinetic energy flux by Lorentz forces.

Figure 2 shows the energy partitioning of our MHD jet solutions for high magnetization

$\sigma = 5000$. We see that only in the case of $q \simeq 0$ the flow remains Poynting dominated also for large radii. In the case of a faster magnetic flux divergence ($q > 0$), the flow accelerates substantially beyond the fast surface, converting more and more Poynting flux into kinetic energy. For the chosen magnetization the kinetic energy becomes substantial only beyond the fast magnetosonic point. Eventually, the energy distribution in the asymptotic flow is in rough equipartition between the kinetic and magnetic contributions. This is consistent with the claim of Begelman & Li (1994), but also with (Newtonian) numerical simulations of jet formation (Ouyed & Pudritz 1997; Fendt & Cemeljic 2002; Ouyed et al. 2003).

3.5. Asymptotic velocity – a modified Michel scaling

Another feature demonstrating the influence of a divergent magnetic field is the correlation (Michel scaling) between asymptotic jet velocity and magnetization (Fig. 3).

As a measure for the asymptotic ($z \rightarrow \infty$) poloidal velocity $u_{p,\infty}$, we have taken the velocity at the $r = 10^4 R_L$. The actual asymptotic value might be a factor of two larger, however, what is important is that the velocity profile saturates significantly beyond 10 – 100 l.c. radii. This implies that, as far as the efficiency of magnetic acceleration is concerned, we do not have to consider the far distant region of the flow.

Figure 3 shows three curves. The lowest curve corresponds to the original Michel scaling $u_{p,\infty} \sim \sigma^{1/3}$ in the case of a magnetic field distribution with $q \simeq 0$. If the magnetic flux decreasing faster ($q > 0$), there is a substantial gain in asymptotic velocity. For the solutions with the decreasing magnetic flux (two upper curves in Fig. 3) we find a *modified Michel scaling*, comparable to an almost linear relation $u_{p,\infty} \simeq A\sigma$, where A depends on the choice of q (this is crucial since large variations of the jet’s Lorentz factor are possible in this solution; see 6.1). For the model parameters discussed here, we find $A \simeq 10^{-1/3}$ for $q = 0.1$ and $A \simeq 10^{-1/5}$ for $q = 0.2$.

Note that the interrelation $u_{p,\infty}(\sigma)$ shown in Fig. 3 essentially provides a link between an asymptotic, “observable” jet parameter (velocity) and a parameter which is intrinsic to the jet origin (magnetization).

3.6. Applicability of the MHD approximation

With the advantage of our approach of knowing the exact solution of the MHD equations along the collimating jet flow, we are able to check self-consistently *a posteriori* whether the *approximation of magnetohydrodynamics* is satisfied within the calculated flow. The problem

is hidden in the fact that for a cold MHD jet one may find arbitrarily high velocities for an arbitrarily high flow magnetization. However, an arbitrarily high magnetization may be in conflict with the intrinsic *MHD condition* under which the solution has been calculated and which requires a sufficient density of charged particles in order to be able to drive the electric current system (Michel 1969). Below a critical particle density the concept of MHD breaks down. As a good measure for this critical density we consider the Goldreich-Julian density n_G (Goldreich & Julian 1969; Lyutikov & Blackman 2001).

Following the notation of equation (8), the particle density n in terms of the Goldreich-Julian density n_G as a function of radius along the magnetic field line is

$$\frac{n(r)}{n_G(r)} = \frac{10^7}{\sigma^2} M_A^{-2}(r) \left(\frac{B_z(r)}{B_z(r_*)} \right)^{-1} \cdot \left(\frac{r_*}{0.05 R_L} \right)^4 \left(\frac{B_*}{10^{12} \text{G}} \right) \left(\frac{R_L}{10^7 \text{cm}} \right) \quad (9)$$

(see Appendix). The index \star denotes a number value at the foot point radius of the magnetic field line r_* . The magnetic field z -component decreases along the opening magnetic flux surfaces while the Alfvén Mach number increases as the jet accelerates. In the Appendix (Fig. 5) we show some example curves of the relative density ($n(r)/n_G(r)$) derived for the jet solutions shown in Fig. 1. Figure 5 demonstrates that the break-down of the MHD concept is critically important rather for highly magnetized jets with weak absolute Poynting flux (implying a low mass flow rate). For all solutions presented in this paper n/n_G stays larger than about 1000.

4. Collimation and the compactness problem

In this section we discuss the structure of the collimating GRB jet. We apply a stationary approach and present axisymmetric solutions of the MHD equations in Kerr metric. Time-dependent general relativistic MHD simulations of jet formation in the literature have failed so far to span time periods of more than some rotational periods.

The axisymmetric magnetic field structure of a stationary collimating MHD jet follows from the solution of the Grad-Shafranov equation (see above). The problem is to obtain a *global* solution which, at the same time, also considers the *local* force-balance. So far, fully self-consistent solutions of the stationary relativistic MHD equations have not yet been able to obtain. The assumption of a self-similar MHD jet is in general a powerful approach in order

to obtain self-consistent MHD jet solutions⁶ (see Vlahakis & Königl (2003) for an application to GRB). However, for the case of relativistic jets this assumption implies a certain angular velocity at the foot point of the field lines $\Omega_F(\Psi) \sim r^{-1}$ (Li et al. 1992) which is in clear contradiction both with the Keplerian rotation of a disk or with the rigid rotation of a central body. Similarly, also the magnetization σ must be flux-independent. It is therefore essential to treat the relativistic MHD jet in a non self-similar, fully two-dimensional approach. So far this has been possible only in the limit of *force-free* force-balance, neglecting the inertial back-reaction of the matter on the field structure (Camenzind 1987; Fendt 1997; Ghosh 2000). It is clear that the previous made comments on a self-similar jet structure become even more valid in the case of a *general relativistic* treatment of MHD jets. Resulting solutions for “self-similar relativistic MHD jets” (Contopoulos 1994; Vlahakis & Königl 2001, 2003) will not be free of these problems.

4.1. Structure of relativistic MHD jets from rotating black holes

Here we summarize the essential steps in calculating the axisymmetric force-balance of relativistic MHD jets (for a detailed discussion see Fendt (1997)). In difference from the previous section we now consider the governing MHD equations in the framework of *general relativity*.

We apply Boyer-Lindquist coordinates in the 3+1 split of space-time around a rotating black hole of mass M and angular momentum per unit mass, $a = J/Mc$ with the line element

$$ds^2 = \alpha^2 c^2 dt^2 - \tilde{\omega}^2 (d\phi - \omega dt)^2 - (\rho^2/\Delta) dr^2 - \rho^2 d\theta^2. \quad (10)$$

t denotes a global time in which the system is stationary, ϕ is the angle around the axis of symmetry, and r, θ are similar to their flat space counterpart spherical coordinates⁷ Here, ω is the “frame dragging” angular velocity of an observer with zero angular momentum (ZAMO), $\omega = (d\phi/dt)_{\text{ZAMO}}$. The lapse function α describes the lapse of the proper time τ in the ZAMO system to the global time t , $\alpha = (d\tau/dt)_{\text{ZAMO}}$.

⁶Still, one has to keep in mind that self-similarity implies further constraints to the solution. (i) It does not allow to include the jet axis in the treatment. (ii) Self-similar jets have an infinite radius. As noted already by Blandford & Payne (1982) the radially self-similar assumption becomes (iii) “increasingly artificial” when the jet has formed at large distances from the disk

⁷The parameters of the metric tensor are defined as usual, $\rho^2 \equiv r^2 + a^2 \cos^2 \theta$, $\Delta \equiv r^2 - 2GMr/c^2 + a^2$, $\omega \equiv 2aGMr/c\Sigma^2$, $\Sigma^2 \equiv (r^2 + a^2)^2 - a^2\Delta \sin^2 \theta$, $\tilde{\omega} \equiv (\Sigma/\rho) \sin \theta$, $\alpha \equiv \rho \sqrt{\Delta}/\Sigma$

We define the axisymmetric magnetic flux Ψ through a loop of the Killing vector $\vec{m} = \tilde{\omega}^2 \nabla \phi$ as

$$\Psi(r, \theta) = \frac{1}{2\pi} \int \vec{B}_P \cdot d\vec{A}, \quad \vec{B}_P = \frac{1}{\tilde{\omega}^2} \nabla \Psi \times \vec{m}, \quad (11)$$

(see Sec. 2.1). The indices P and T denote the poloidal and toroidal components of a vector. Similar to Eq. (11) the total poloidal electric current is defined by $I = - \int \alpha \vec{j}_P \cdot d\vec{A} = -\frac{c}{2} \alpha \tilde{\omega} B_T$. In a force-free magnetosphere with $0 = \rho_c \vec{E} + \frac{1}{c} \vec{j} \times \vec{B}$ the poloidal electric current is parallel to the poloidal magnetic field $\vec{B}_P \parallel \vec{j}_P$ and is a conserved quantity along the magnetic flux surfaces, $I = I(\Psi)$.

The axisymmetric force-balance perpendicular to the magnetic field is described by the Grad-Shafranov equation (hereafter GSE). In the limit of highly relativistic (i.e. highly magnetized) jets, inertial forces have a negligible influence on the *structure* of the magnetosphere and we may apply the force-free limit of the GSE,

$$\tilde{\omega} \nabla \cdot \left(\alpha \frac{1 - (\tilde{\omega}/\tilde{\omega}_L)^2}{\tilde{\omega}^2} \nabla \Psi \right) = -\frac{g_I}{2} \frac{1}{\alpha \tilde{\omega}} \frac{dI(\Psi)}{d\Psi}. \quad (12)$$

For simplicity, differential rotation of the jet basis has been neglected, $\Omega_F(\Psi) = \text{const.} = \Omega_F$. The two light surfaces are located at the radial position $\tilde{\omega}_L = (\pm \alpha / (\Omega_F - \omega))^{1/2}$. The + sign holds for the outer light surface with $\Omega_F > \omega$, while the – sign stands for the inner light surface, where $\Omega_F < \omega$. The asymptotic radius of the outer light surface ($\tilde{\omega}_L$ for $z \rightarrow \infty$), the light cylinder, is denoted by R_L . Normalizing the GSE (12) using $\tilde{\omega} \rightarrow R_L \tilde{\omega}$; $\nabla \rightarrow (1/R_L) \nabla$; $\Psi \rightarrow \Psi_{\max} \Psi$ and $I \rightarrow I_{\max} I$ is numerically advantageous, but also provides insight in the physical characteristics of the solution. The coupling constant g_I measures the strength of the source term of the GSE,

$$g_I = \frac{4I_{\max}^2 R_L^2}{c^2 \Psi_{\max}^2} = 0.5 \left(\frac{I_{\max}}{10^{15} \text{A}} \right)^2 \left(\frac{R_L}{10^7 \text{cm}} \right)^2 \left(\frac{\Psi_{\max}}{10^{21} \text{Gcm}^2} \right)^{-2}. \quad (13)$$

Basically, g_I determines the strength of the electric current I_{\max} . A high coupling constant corresponds to a strong poloidal electric current (respectively a strong toroidal magnetic field) and therefore implies a strong jet collimation. Note that the coupling between the source term and the poloidal field structure considers *only electromagnetic* quantities. The solution is, however, calculated in Kerr metric, and considers also gravity. The link between the two governing length scales defined in the problem – the asymptotic light cylinder and the gravitational radius – is made by choosing Ω_F in terms of the black hole rotation Ω_H (see below).

Equation (13) applies parameter estimates as discussed above for GRB jets launched by black hole accretion disks. The maximum poloidal electric current in the disk-jet system is

given by the disk equipartition field strength. For an advection dominated disk (see Eq. (4)) we have $B_{\text{T}}^{\text{max}} \lesssim B_{\text{eq}} \simeq 10^9 \text{G}$ and $I_{\text{max}} \lesssim 3 r_{\text{g}} B_{\text{T}} c / 2 \simeq 10^{15} \text{A}$. Since $B_{\text{P}}^{\text{max}} \lesssim B_{\text{T}} \simeq B_{\text{eq}}$ in the disk, we derive a maximum magnetic flux from the disk $\Psi_{\text{max}} \lesssim \pi (3r_{\text{g}})^2 B_{\text{P}}^{\text{max}} \simeq 10^{21} \text{G cm}^2$. The expression for g_{I} can be further simplified considering that the light cylinder radius in Eq. (13) is governed by the rotation of the jet foot point Ω_{F} . As both $B_{\text{T}}^{\text{max}}$ and $B_{\text{P}}^{\text{max}}$ are limited by B_{eq} as a function of radius, we finally obtain

$$g_{\text{I}} = 0.6 \left(\frac{B_{\text{T}}^{\text{max}}}{B_{\text{P}}^{\text{max}}} \right)^2 \left(\frac{r_{\star}}{6r_{\text{g}}} \right). \quad (14)$$

For the case of hyper-accreting disks discussed above, the limiting equipartition field strength constrains the poloidal and toroidal field equivalently. As a consequence, the coupling g_{I} remains the same.

4.2. Example solution for a fully collimated GRB jet

Here we present an example solution for the stationary axisymmetric force-free magnetic field structure of GRB jets calculated from the Grad-Shafranov equation (12). The GSE is solved applying the method of finite elements. This allows to consider the complex geometrical structure of the black hole - disk - jet system. Details of the method of solution are discussed elsewhere (Fendt 1997). We summarize the following characteristics of the solution.

- The shape of the collimating outer jet boundary is not known a priori. It is determined by the internal structure of the jet and is particularly constrained by the regularity condition along the outer light surface (i.e. a smooth transition of the magnetic field lines).
- The “free function” $I(\Psi)$ in the GSE source term is chosen from the analytical solution of an asymptotic jet in perfect collimation.
- The interrelation between the two characteristic length scales of the solution, the asymptotic light cylinder and the gravitational radius – hence, the link between electrodynamics and gravity – is made by choosing the angular rotation $\Omega_{\text{F}}(\Psi)$. Here, $\Omega_{\text{F}} = 0.4\Omega_{\text{H}}$ corresponding to the Keplerian rotation at the marginally stable orbit. With that $R_{\text{L}} = 10r_{\text{g}}$ for $a = 0.8$.
- Other parameters are the magnetic flux from the black hole in terms of the total flux, $\Psi_{\text{BH}}/\Psi_{\text{max}} = 0.2$, and the profile of the disk magnetic flux distribution.

Figure 4 shows the resulting structure of the collimating magnetic flux surfaces. The solution extends from the inner light surface to the asymptotic regime of a fully collimated jet. We find a perfect collimation of the asymptotic jet in agreement with analytical models of (Appl & Camenzind 1993). We find a rapid collimation of the outflow into a cylindrical shape within $50r_g$ distance from the central black hole. The expansion rate (asymptotic jet radius in respect to the jet foot point radius) is about 10. The asymptotic jet radius is 5 l.c. radii. Due to the numerical resolution we do not obtain solutions with larger jet radius.

Whether the jet is self-collimated by magnetic tension or pressure collimated by an ambient medium cannot be answered by this approach.

An interesting fact is that the flux surfaces emerging from the black hole (i.e. from the inner light surface in our approach) asymptotically partly intersect with the outer light surface. This implies that the mass load in the jet provided by the accretion disk is predominantly in the outer layers of the jet at radii $r > R_L$. Here, we expect the high velocities calculated in the previous section together with a strong toroidal magnetic field. The inner part of the jet with flux surfaces emerging from the black hole, should be dilute of matter, i.e. we have a hollow jet stream. This part of the jet may be powered by the electromagnetic interaction with the black hole itself (Blandford-Znajek mechanism).

The strength of the coupling is similar to the case of active galactic nuclei (AGN). As the coupling constant Eq.(13) measures the strength of the collimating toroidal magnetic field strength in terms of the de-collimating effects poloidal field and rotation⁸. Therefore, we may expect a similar structure of the jet magnetosphere in both examples. A strong coupling implies efficient collimation; we find that collimation angles as low as $0^\circ - 5^\circ$ can be achieved with proper tuning of parameters. From AGN jets we know that they are well collimated with asymptotic jet radii up to of about $100 R_L$. Just from the similarity of the coupling constant we might expect the same scaling also for jets in GRB's. To calculate such large jet radii is, however, beyond the capability of our numerical code.

5. The “bottle-neck” instability for highly magnetized jets

In the previous sections we have presented stationary solutions for highly magnetized MHD jets – the flow dynamics along the collimating magnetic field and the axisymmetric magnetic field structure. Our time scale estimates (Eq.7) indicate that the stationary approach may indeed be applied when considering the jet formation region. Nevertheless, it is

⁸Note that the coupling constant corresponds to the inverse magnetization for force-free jets

clear that the GRB itself must be the consequence of a time-dependent process. The current picture of GRB invokes highly relativistic shells moving with different speed, catching up with each other by forming a highly energetic shock front – the gamma ray burst (Piran 1999).

From our MHD solutions we have found indication of a possible excitation mechanism for a flow instability. This instability essentially relies on (i) a *high magnetization* and (ii) a *re-collimation* of the governing magnetic flux tube. The solutions discussed in Sec. 3 have been calculated for a *decreasing* function Φ along the jet corresponding to a increasing opening of the flux tube. However, the two-dimensional jet magnetic field structure as presented in Sec. 4 shows an interesting property. The global jet collimates into a cylindrical shape with the single flux surfaces turning from an initially conical outflow close to the disk into an alignment parallel to the jet axis. This implies a *re-collimation of the single flux tube* – easily visible when comparing the width of the flow channel along the outer flux surfaces (see also Fendt & Camenzind (1996)). The maximum width is typically located in the region of the strongest curvature at a distance of several R_L from the central source.

Solving the wind equation by considering a re-collimation of the flux tube we find that *no stationary wind solutions exists beyond the radius where re-collimation happens*. We cannot directly answer the question what exactly happens there as this is beyond our stationary approach. For comparison, one may think of the earth magnetosphere reflecting solar wind particles from the polar region or the more general picture of a “magnetic bottle” of converging magnetic field lines.

In the appendix we show a typical MHD wind solution as discussed in Sec. 3, but modified for the re-collimation feature by prescribing an increasing magnetic flux tube function Φ beyond a certain radius. In this example we applied a cosine-like recollimation of the flux tube $\Phi(r) \sim r^{-0.2}$ within a certain radius range beyond $r > 50r_A \simeq 50R_L$ (see Eq. B1). Figure 6 shows an example velocity distribution along the field line for different magnetization. For high magnetization the magnetic field is strong enough to brake the matter sufficiently. The exact dynamical behavior depends on the parameters of the wind solution. Essentially, the re-collimation leads to a deceleration of the wind flow before the stationary solution ceases to exist. Applying a spatially limited region of re-collimation, e.g. a sinusoidal variation of $\Psi(r)$ between two radii, there may exist a unique *stationary* flow solution which can be decelerated below the magnetosonic velocity. However, in reality such a unique combination of field distribution and mass flow rate may not exist.

Therefore, we propose the above mentioned indication of a “bottle-neck” instability as a generic reason for the velocity variation and the formation of shock waves in GRB. This instability is working predominantly in the outer layers of the jet and in the collimation

regime at distances of several l.c. radii from the central object.

The onset of the instability depends on the details of the flow propagation. However, in general, the essential conditions are *strong magnetization* and *re-collimation*. Due to the Michel scaling, this corresponds in particular to high Lorentz factors as present in jets of GRBs. In our example model we compare magnetizations of $\sigma = 10, 1000, 5000$ and a certain sinusoidal variation of the flux tube function (see Appendix). It can be seen that for low magnetization a stationary solution exists from the jet foot point to the asymptotic regime. For higher magnetization, the stationary solution ceases to exist at a certain radius. For the parameter choice applied here, we do not find a stationary flow domain around the location of local maximum re-collimation. In the case of further recollimation, no stationary wind solution will be found beyond this radius. In our case, with an again increasing size of the flux tube, stationary solution can be found beyond the non-stationary regime. This, however, has no consequence as the jet flow has become non-stationary already. *We note that it is not straightforward to estimate the exact location of the radius where the instability occurs. However, it seems to occur at large enough radii to assume that it is beyond the Compton photosphere.*

6. Ultra-relativistic MHD jets in the GRB picture

6.1. Varying Lorentz factor and internal shocks

Mass-load

Variations in the Lorentz factor of $10 - 1000$ ($10^2 < \Gamma < 10^5$) as suggested by the GRB internal shock model are hard to obtain from the original Michel scaling. In fact, $u_{p,\infty} \sim \dot{M}_{\text{jet}}^{-1/3}$ would imply a variation in the mass load by several orders of magnitude more. The existence of a modified Michel scaling as described in §3.5 (see Fig. 3) leaves the possibility of having a substantial change on the Lorentz factor by the variation of the initial flow magnetization. A variation in the jet magnetization can be caused by a change in the mass injection rate from the accretion disk into a jet with temporarily constant magnetic field implying $u_{p,\infty} \sim \dot{M}_{\text{jet}}^{-1}$. It is interesting to note that these variations are directly induced by conditions at the source pending contamination by the surrounding material as discussed next.

Ambient mass-entrainment

One would expect parts of the jet to be contaminated by the ambient material (Daigne & Mochkovitch 2000) as to cause local variation to the intrinsic Lorentz factors (as given

by the disk mass loading or magnetization). In fact, it is likely that the variations in the Lorentz factors are induced by a combination of varying mass-load and mass-entrainment. This would result in a multiple shock mergers inducing GRBs (as in the internal shock scenario) which can be seen if mass entrainment occurs mainly beyond the compactness radius.

6.2. Magnetic energy dissipation

It is argued that, for models of internal shocks in GRBs to successfully reproduce the GRB temporal features, different shells of matter should have a comparable energy and their different Lorentz factors should arise due to modulation of the accelerated mass (Piran (2001) and references therein). In MHD jets, the energy (mainly magnetic at the base of the flow) is roughly constant as the magnetization is not expected to vary much. A variable mass-load combined with the entrained mass, as we have said, offers the modulation needed to account for the wide range in the Lorentz factors⁹. By itself, such a variable source is not enough to explain the variable light curves since magnetic energy dissipation mechanisms will not necessarily be efficient or adequate in reproducing the GRB temporal structure¹⁰. For the Crab Pulsar wind in which energy is transported predominantly as Poynting flux, the fluctuating component of the magnetic field in such a flow can in principle be dissipated by magnetic reconnection and used to accelerate the flow (Kirk & Skjæraasen 2003). In our model, such mechanisms might be at play as a result of the “bottle-neck” instability. A conversion of the fraction of the energy of the accelerated particles into radiation is interesting within the GRB context. The pulsation of the emitted radiation in our picture, as we have argued above, would be linked to the variation in the accretion rate at the source. We note however that it is not yet clear how much of the magnetically dissipated energy can be seen in the form of γ -rays (Spruit et al. 2001).

6.3. Collimation and polarization

The results from §4 suggest that ultra-relativistic MHD jets are highly collimated. Extrapolating from what we know in the case of AGN jets this implies that collimation angles

⁹This may also lead to a narrow range in the Lorentz factor distribution as part of the jet with higher Lorentz values would in principle induce higher entrainment; a notion which remains to be confirmed.

¹⁰Dissipation in shocks (internal and external shocks) is fundamentally different from magnetic energy dissipation in MHD outflows where non-thermal electron distributions is not guaranteed.

as small as $0^\circ - 5^\circ$ are feasible. Such an efficiency in collimation is a statement that the jet is asymptotically dominated by the *toroidal magnetic field* component (§3.3). This may have important implications e.g. for the magnetic field distribution in the asymptotic shocks and for the interpretation of the polarization structure in the afterglow observations.

7. Summary

We studied ultra-relativistic MHD jets in the context of GRBs. We have presented stationary solutions for the governing MHD equations considering the axisymmetric structure of the collimating jet and the acceleration of matter by the magnetic field. Special and general relativistic effects have been taken into account.

Lorentz factors up to 3000 can be obtained for sufficient strong jet magnetization. The advantage of our approach of actually solving the governing MHD equations is that we can prove *a posteriori* the applicability of MHD itself by comparing the matter density with the Goldreich-Julian density along the jet flow. The asymptotic jet magnetic field is dominated by the toroidal component. The energy distribution within the asymptotic jet is almost in equipartition between magnetic and kinetic energy.

For the structure of the axisymmetric MHD jet we find a rapid collimation to almost perfect collimation within a distance from the black hole of about half the jet radius (of 5 light cylinder radii in this example).

Among the features that are crucial to standard models of GRBs, are (i) the modified Michel scaling ($u_{p,\infty} \sim \dot{M}_{\text{jet}}^{-1}$) which allows for a plausible variation in the Lorentz factor by variations in the source parameters such as the disk magnetization and/or mass-loading; (ii) the high degree of collimation ($\theta \sim 0^\circ - 5^\circ$) which is within the range of values derived from breaks of afterglow light curves. We isolated a jet instability that develops at extreme Lorentz factors. This instability which seems to arise at large radii, if it occurs beyond the compactness radius, would result on an optically thin emission once its associated magnetic field is dissipated. We expect different magnetic field configurations to lead to different dynamics (e.g. asymptotic profiles, dissipation efficiency). This, in principle, could reproduce the large diversity and duration range of GRBs.

Among the open questions are the extreme magnetic fields required, and the effect of baryon contamination (via mass-entrainment) on the distribution of the Lorentz factors. It is also not clear at this stage why and how the engine (the underlying hole-disk system here) should stop for several dozens seconds before bursting again as seen in GRBs.

A. Applicability of the MHD concept

As discussed above highly relativistic jets must be strongly magnetized (Michel (1969); Camenzind (1986); Fendt & Camenzind (1996); see Sec.2.4). Magnetohydrodynamic jets live from magnetic to kinetic energy conversion. More kinetic energy per fluid element can be delivered for jets with correspondingly strong magnetic field, or low mass flow density, respectively. On the other hand, the *MHD concept* itself requires a minimum density of charged particles in order to allow for electric currents in the flow. The jet flow mass density naturally decreases along the flow as the jet originates in a very small region close to the central source and first expands in almost radial direction before it collimates into a narrow beam. When the flow density is below the critical density at the MHD radius r_{MHD} , the MHD assumption breaks down. With our model approach, we may determine self-consistently the possible breakdown of the MHD conception as our MHD wind solution delivers all the dynamical and electromagnetic properties of the flow.

Melatos & Melrose (1996) quantify the range of validity for *ideal* MHD, $\vec{E} + \vec{v} \times \vec{B} = 0$, by inspecting the one-fluid equations for a cold, neutral plasma. They consider the generalized Ohm's law for fluctuations of time scales τ on characteristic length scales λ in the magnetohydrodynamic quantities. In the end, there are four constraints for ideal MHD. First, it is required that $j \ll nev$ and $\rho_c v \ll j$ with the charge density ρ_c . If the conduction current is dominating the displacement current, Maxwell's equations imply that for MHD $(4\pi j\tau/E) \simeq (c\tau/\lambda)^2$. With the relation

$$\frac{\Gamma c^2}{\omega_0^2 \lambda^2} \max\left(1, \frac{\lambda}{\tau v}, \frac{\tau v}{\lambda}\right) \ll 1 \quad (\text{A1})$$

(with $\omega_0 \equiv \sqrt{4\pi ne^2/m_p}$) Ohm's law actually reduces to $\vec{E} + \vec{v} \times \vec{B} \simeq 0$. In the case of a pulsar wind with $\lambda \simeq R_L$, $\omega \simeq \Omega_\star = \Omega_F$ and $\tau \simeq \omega^{-1} = R_L/c$, Eq. (A1) takes the form $\Gamma\omega^2 \ll \omega_0^2$ which is equivalent to the estimate of Michel (1969). For the Crab pulsar the MHD radius is located at $r_{\text{MHD}} \simeq 10^5 R_L$ (Melatos & Melrose 1996).

A similar criterion for the applicability of MHD is a matter density above the *Goldreich-Julian charge density* (Goldreich & Julian 1969; Michel 1969). The Goldreich-Julian particle density along a magnetic flux surface $\Psi(r, z)$ is

$$n_G = -\frac{(\nabla\Psi \cdot \nabla)(r^2\Omega_F)}{4\pi c e r^2} = \frac{B_z(r; \Psi)}{2\pi e c R_L}, \quad (\text{A2})$$

and is not negligible for rapid (relativistically) rotating magnetospheres. Again, a particle density below the Goldreich-Julian density indicates that not enough charges are available to carry the electric current. From Eq. (A2) we see that if the particle density profile decreases

faster than the B_z component, there may exist a critical distance r_{MHD} where the matter particle becomes lower than the Goldreich-Julian density.

Usov (1994) has applied this approach in order to model GRBs generated by millisecond magnetars of $3 \times 10^{15}\text{G}$ dipolar field strength,

$$n_{\text{G}} = 4 \times 10^{16} \frac{r_{\star}}{r} \left(\frac{B_{\star}}{3 \times 10^{15}\text{G}} \right) \left(\frac{\Omega_{\text{F}}}{10^4\text{s}^{-1}} \right)^3 \text{cm}^{-3}. \quad (\text{A3})$$

In the case of a leptonic plasma wind Usov derives a critical distance $r_{\text{MHD}} \simeq 10^{13}\text{cm}$ for the given stellar magnetic field strength and field distribution and the rotation rate ($\Omega_{\text{F}} = 10^4\text{s}^{-1}$). It is, however, another question to extrapolate these variables over more than six orders of magnitude in distance from the star to the region where the critical radius is located in this model. A similar approach has been applied in the context of ‘‘Poynting-dominated’’ outflows in GRBs (Lyutikov & Blackman 2001), assuming a certain magnetic field and density distribution. In this model, large-amplitude electromagnetic waves break at the MHD radius located at about 10^{14}cm while accelerating particles to ultra-relativistic speed.

In difference to the previous work, in our paper we calculate the solution of the relativistic MHD wind equation from the jet basis to the asymptotic regime providing us with a set of dynamical properties of the flow. In particular, this allows us to check self-consistently (but a posteriori) the consistency of our solutions with the MHD conception. With that we may also compare different jet geometries – rapid or weak collimation – and may constrain the parameters of the jet mass loading and the magnetic field distribution. We derive an expression for the matter particle density from the definition of the Alfvén Mach number,

$$M_{\text{A}}^2 = \frac{4\pi\mu n' u_{\text{p}}^2}{B_{\text{p}}^2} \quad (\text{A4})$$

with the proper particle density n' , the gas entropy μ and the poloidal velocity $u_{\text{p}} \equiv \Gamma v_{\text{p}}/c$ (Camenzind 1987; Fendt & Camenzind 1996). Re-writing Eq. (A4) gives the proper particle density along the magnetic field line as a function of the Alfvén Mach number,

$$n' = \frac{1}{4\pi} \frac{\Psi_{\text{D}}^2}{m_{\text{p}} c^2 \sigma^2 R_{\text{L}}^2 M_{\text{A}}^2}. \quad (\text{A5})$$

Relating that to the Goldreich-Julian density Eq. (A2), we find Eq. (9). As the Alfvén Mach number generally increases faster than the z-component of the magnetic field decreases along the flow, the ratio (n'/n_{GJ}) will decrease. In Fig. 5 we show the profile of the density ratio for four of the example wind solutions presented in Fig. 1. For all four cases the mass flow density stays above the Goldreich-Julian density. The MHD jet parameters are the magnetization

$\sigma = 1000, 5000$ and the foot point magnetic field strength of $B_p = 10^9\text{G}, 10^{12}\text{G}$. In particular, we find that the density ratio approaches a constant value $n'/n_{\text{GJ}} \gtrsim 100$ for large radii. This reflects the fact of a *jet collimation*. For a further (substantial) expansion of the jet flow for these choice of initial parameters, the mass density would become under critical.

B. Recollimation – the “bottle neck” instability

Here we show example solutions of the MHD wind equation for the case of a local re-collimation flux tube function $\Phi(r)$. For this purpose we modified the decreasing magnetic flux tube function $\Phi(r)$ by simply adding a cosine shape increase within a certain radius range along the jet. For the solutions presented in Fig. 6 we have prescribed

$$\begin{aligned} \Phi(r) &\sim r^{-0.2} \quad \text{for } r < 50 r_A \\ \Phi(r) &\sim r^{-0.2} \left(1 + 1.25 \left(1 - \cos\left(\frac{r - 50}{2000}\pi\right) \right) \right) \\ &\quad \text{for } 50 r_A < r < 2050 r_A \\ \Phi(r) &\sim r^{-0.2} (1 + 1.25 (1 - \cos \pi)) \quad \text{for } r > 2050 r_A \end{aligned} \tag{B1}$$

We have computed the wind solution for several different magnetizations and otherwise equal parameters. Figure 6 shows that for low magnetization ($\sigma = 10$) the stationary wind solution reaches from the foot point into the asymptotic domain. For higher magnetization ($\sigma = 1000, 5000$) no stationary solution can be found along a certain radial range around the point of (local) maximum re-collimation (see $\Phi(r)$ -plot).

REFERENCES

- Appl, S., & Camenzind, M. 1993, A&A, 274, 699
 Begelman, M. C., & Li, Z.-Y. 1994, ApJ, 426, 269
 Blandford, R. D., & Payne, D. G. 1982, MNRAS, 199, 883
 Camenzind, M. 1986, A&A, 162, 32
 Camenzind, M. 1987, A&A, 184, 341
 Camenzind, M., 1989, Hydromagnetic flows from rapidly rotating compact objects and the formation of relativistic jets, in: Accretion disks and magnetic fields in astrophysics, G. Belvedere (ed), Kluwer, Dordrecht, p. 129-143

- Castro-Tirado, A. J., et al. 1999, *Science*, 283, 2069
- Contopoulos, J. 1994, *ApJ*, 432, 508
- Daigne, F., & Mochkovitch, R. 2000, *A&A*, 358, 1157
- Fendt, Ch. 1997, *A&A*, 319, 1025
- Fendt, Ch., & Camenzind M. 1996, *A&A*, 313, 591
- Fendt, Ch., & Greiner, J. 2001, *A&A*, 369, 308
- Fendt, Ch., & Cemelijic, M. 2002, *A&A*, 395, 1045
- Ghosh, P. 2000, *MNRAS*, 315, 207
- Goldreich, P., & Julian, W. H. 1969, *ApJ*, 157, 869
- Goodman, J. 1986, *ApJ*, 308, L47
- Kirk, J. G., & Skjæraasen, O. 2003, *ApJ*, 591, 366
- Koide, S., Meier, D.L., Shibata, K., & Kudoh, T. 2000, *ApJ*, 536, 668
- Kudoh, T., Matsumoto, R., & Shibata, K. 1998, *ApJ*, 508, 186
- Kulkarni, S. R., et al. 1999, *Nature*, 398, 389
- Li, Z.-Y., Chiueh, T., & Begelman, M.C. 1992, *ApJ*, 394, 459
- Li, Z.-Y. 1993, *ApJ*, 415, 118
- Lyutikov M., & Blackman E.G. 2001, *MNRAS*, 321, 177
- Michel, F. C. 1969, *ApJ*, 158, 727
- Melatos A., & Melrose D. B. 1996, *MNRAS*, 279, 1190
- Mészáros, P., & Rees, M. J. 1993, *ApJ*, 418, L59
- Mészáros, P., & Rees, M. J. 1997, *ApJ*, 482, L29
- Mészáros, P. 2002, *ARA&A*, 40, 137
- Narayan, R., Mahadevan, R., & Quataert, E. 1998, Advection-dominated accretion around black holes, in: *Theory of Black Hole Accretion Disks*, M. Abramowicz et al. (eds), Cambridge University Press, p.148

- Ouyed, R., & Pudritz, R. E. 1997, *ApJ*, 482, 712
- Ouyed, R., Clarke, D. A., & Pudritz, R. E. 2003, *ApJ*, 582, 292
- Paczyński, B. 1990, *ApJ*, 348, 485
- Papathanassiou, H., & Meszaros, P. 1996, *ApJ*, 471, L91
- Piran, T. 1999, *Physics Reports*, 314, 757
- Piran, T., & Nakar, E. 2001, How to construct a GRB engine, in: *Proceedings of Compact Stars in the QCD Phase Diagram (CSQCD)*, (www.slac.stanford.edu/econf/C010815), p. 182-193, 2002
- Popham, R., Woosley, S. E., & Fryer, C. 1999, *ApJ*, 518, 356
- Pudritz, R. E., & Norman, C. A. 1983, *ApJ*, 274, 677
- Rees, M. J., & Mészáros, P. 1994, *ApJ*, 430, L93
- Sari, R., & Piran, T. 1997, *MNRAS*, 287, 110
- Shemi, A., & Piran, T. 1990, *ApJ*, 365, 55
- Spruit, H.C., Daigne, F., & Drenkhahn, G. 2001, *A&A*, 369, 694
- Stanek, K. Z., Garnavich, P. M., Kaluzny, J., Pych, W., & Thompson, I. 1999, *ApJ*, 522, L39
- Tavani, M. 1996, *ApJ*, 466, 768
- Thompson, C. 1994, *MNRAS*, 270, 480
- Thompson, C., & Madau, P. 2000, *ApJ*, 538, 105
- Usov, V. V. 1994, *MNRAS*, 267, 1035
- Vlahakis, N., & Königl, A. 2001, *ApJ*, 560, 145
- Vlahakis, N., & Königl, A. 2003, *ApJ*, 596, 1104
- Wijers, R. A. M. J., Rees, M. J., & Meszaros, P. 1997, *MNRAS*, 288, L51

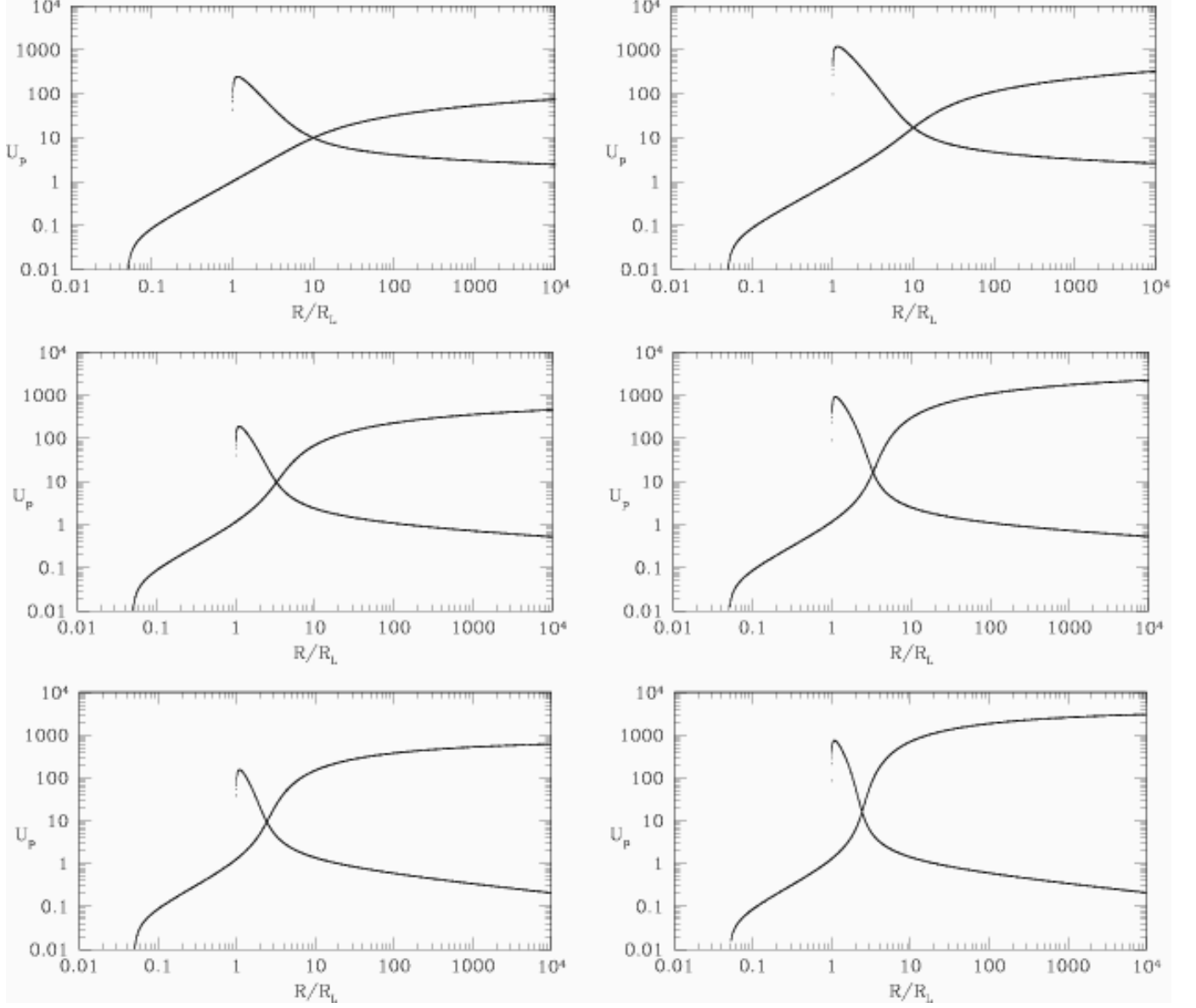


Fig. 1.— Relativistic MHD wind/jet solution. Poloidal velocity u_p along the magnetic field line. Parameter: $\sigma = 1000$ (left), $\sigma = 5000$ (right), Parameter: $\Phi(r) \sim r^{-q}$, $q = 0.01$ (top), $q = 0.1$ (middle). $q = 0.2$ (bottom).

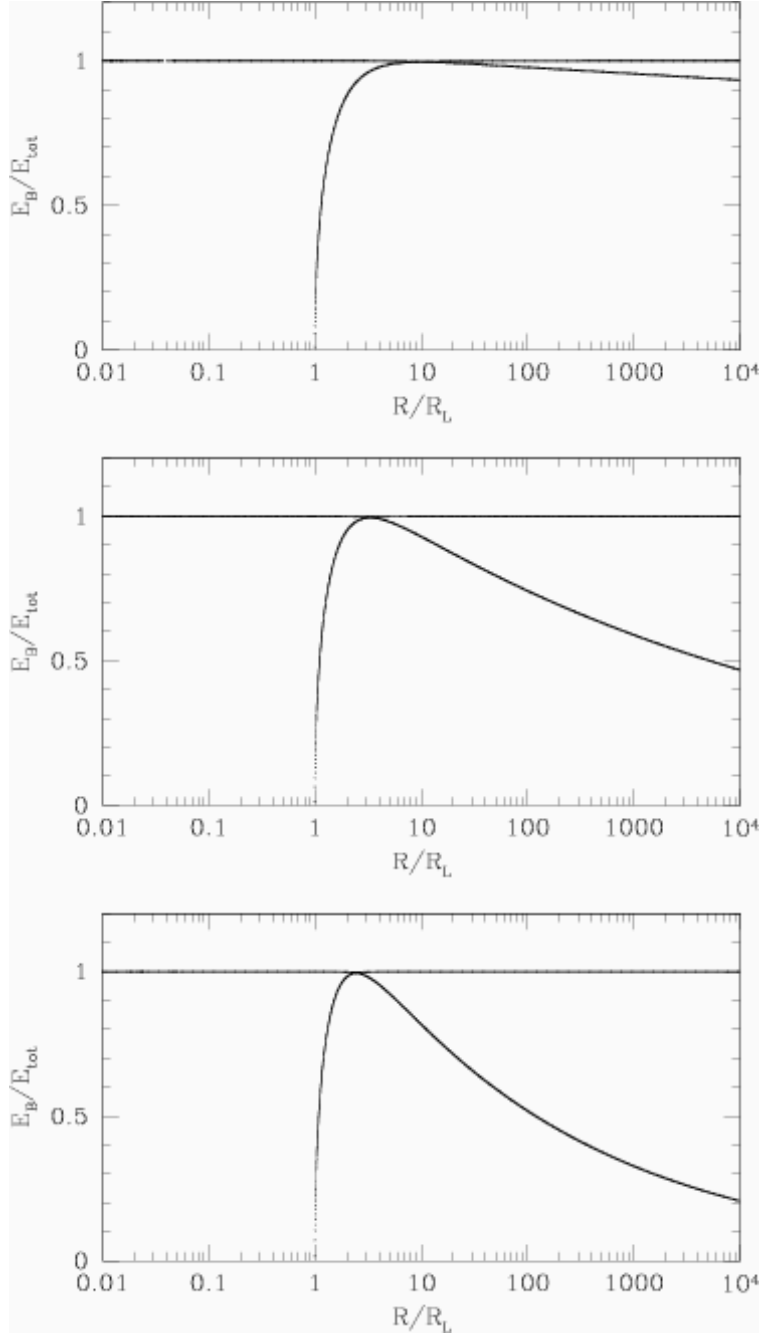


Fig. 2.— Relativistic MHD wind/jet solution. Magnetic energy in terms of total energy as a function of radius along the magnetic field line. Note the fast magnetosonic point as intersection of both curves. Parameter: $\sigma = 5000$, $\Phi(r) \sim r^{-q}$, $q = 0.01, 0.1, 0.2$ (from *top* to *bottom*).

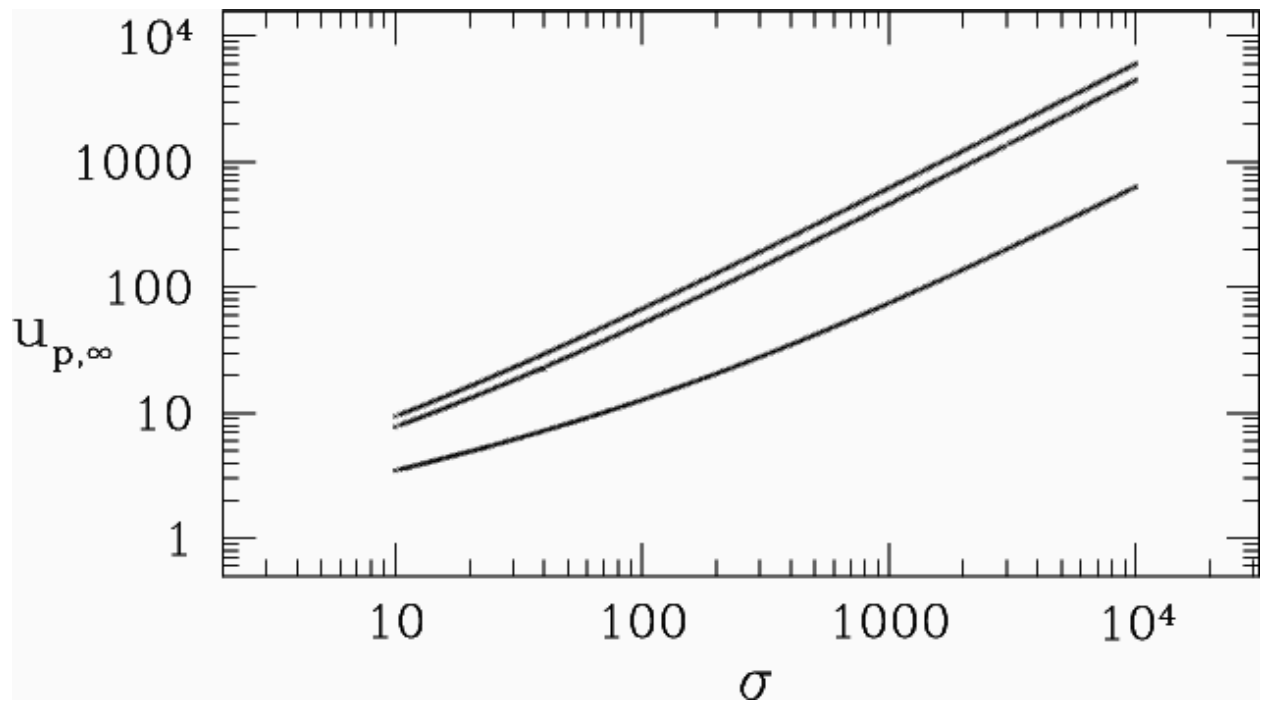


Fig. 3.— Relativistic MHD jet solution. Modified Michel scaling $u_{p,\infty}(\sigma)$ for a different choice of the magnetic field distribution $\Phi(r; \Psi) \sim r^{-q}$ with $q = 0.2$ (*top curve*), $q = 0.1$ (*middle curve*), $q = 0.01$ (*bottom curve*).

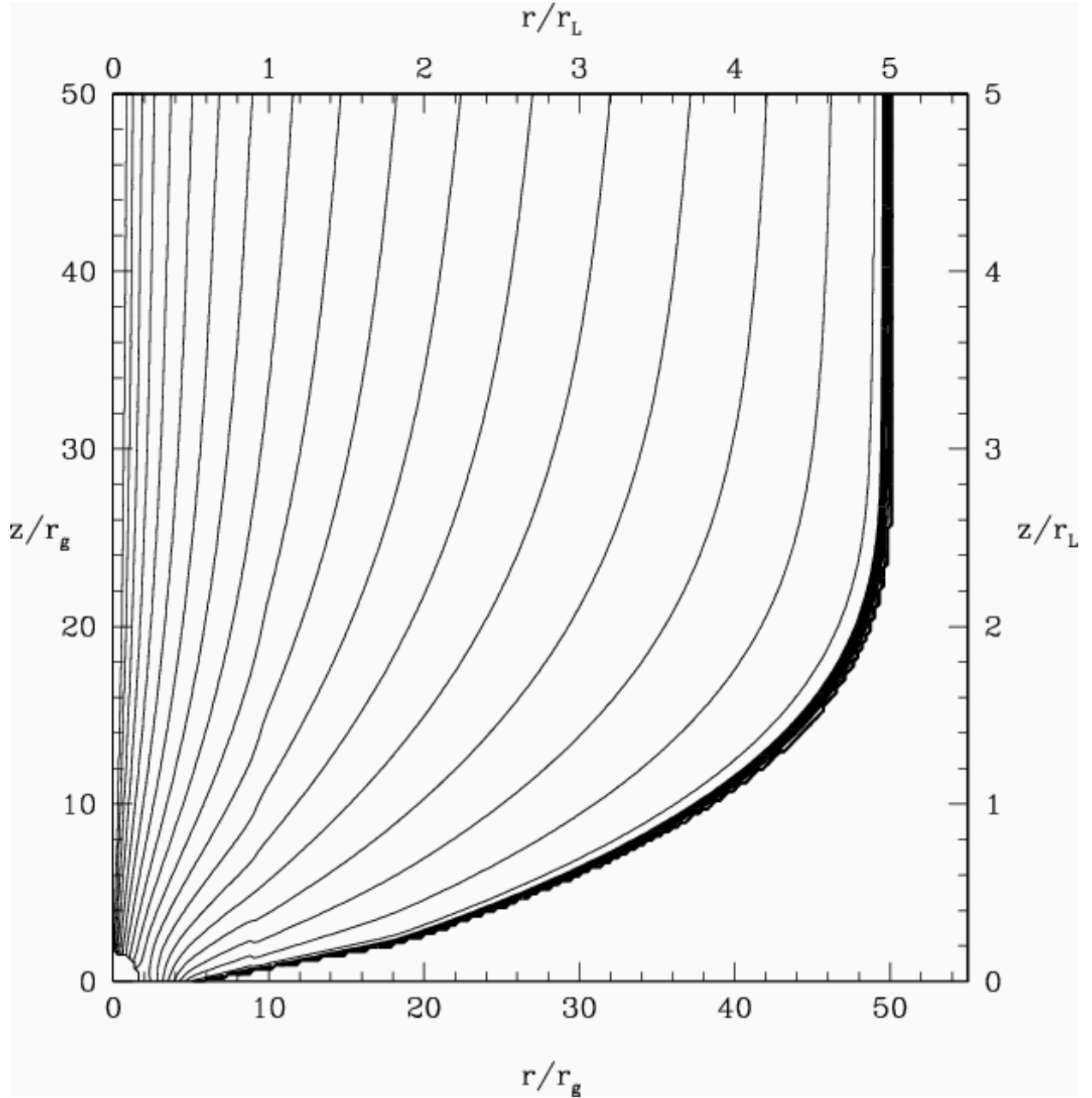


Fig. 4.— The axisymmetric magnetic field structure of a jet from a rotating black hole as solution of the Grad-Shafranov equation in Kerr metric $\Psi(r, z)$. The jet originates within $5r_g$ of the accretion disk. Parameters: BH angular momentum parameter $a = 0.8$, coupling constant $g_I = 0.717$, jet radius $r_{\text{jet}} = 50 r_g$, asymptotic light cylinder $R_L = 10 r_g$, black hole magnetic flux $\Psi_{\text{BH}} = 0.1 \Psi_{\text{total}}$. By prescribing g_I , r_{jet} and the disk flux distribution, the shape of the collimating jet boundary (*thick curve*) is determined by the regularity condition at the light surface. The inner boundary is the inner light surface around the ergosphere (white hemisphere).

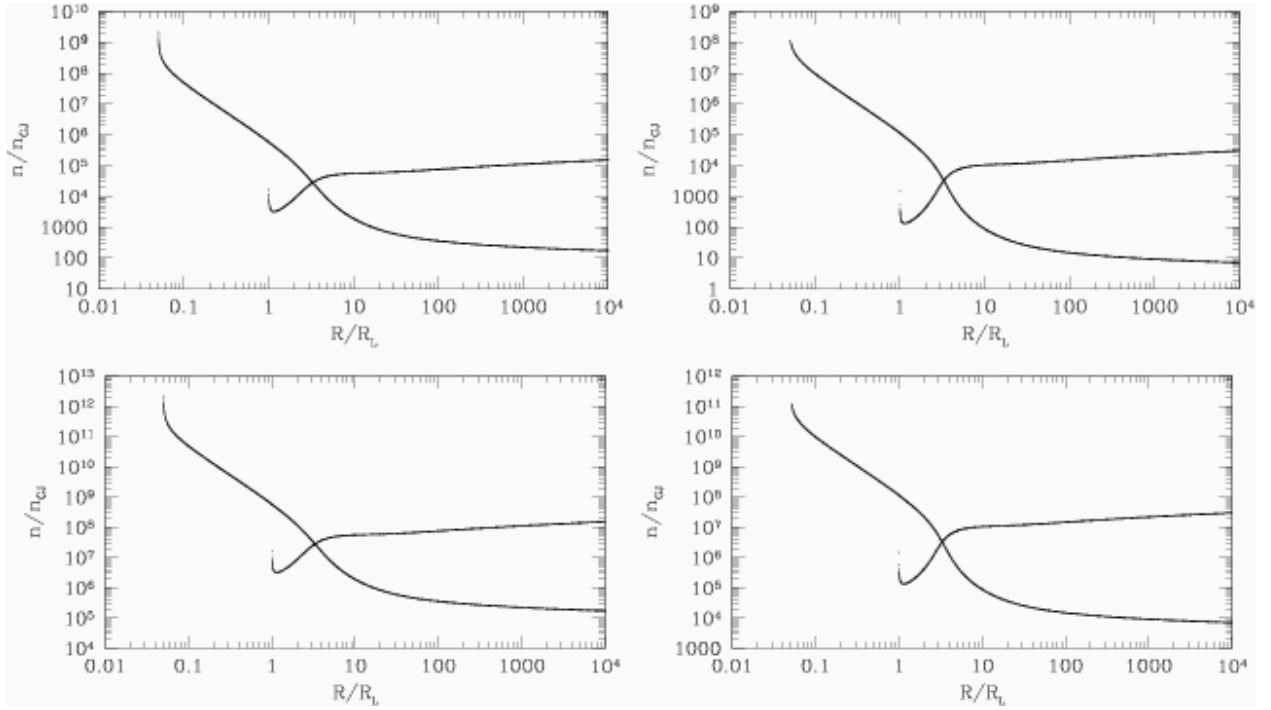


Fig. 5.— Relativistic MHD wind/jet solution. Particle density in terms of Goldreich Julian particle density as a function of radius along the magnetic field line. Parameter: $\sigma = 1000$ (left), $\sigma = 5000$ (right), initial magnetic field strength $B_{z,\star} = 10^9\text{G}$ (top), $B_{z,\star} = 10^{12}\text{G}$ (bottom).

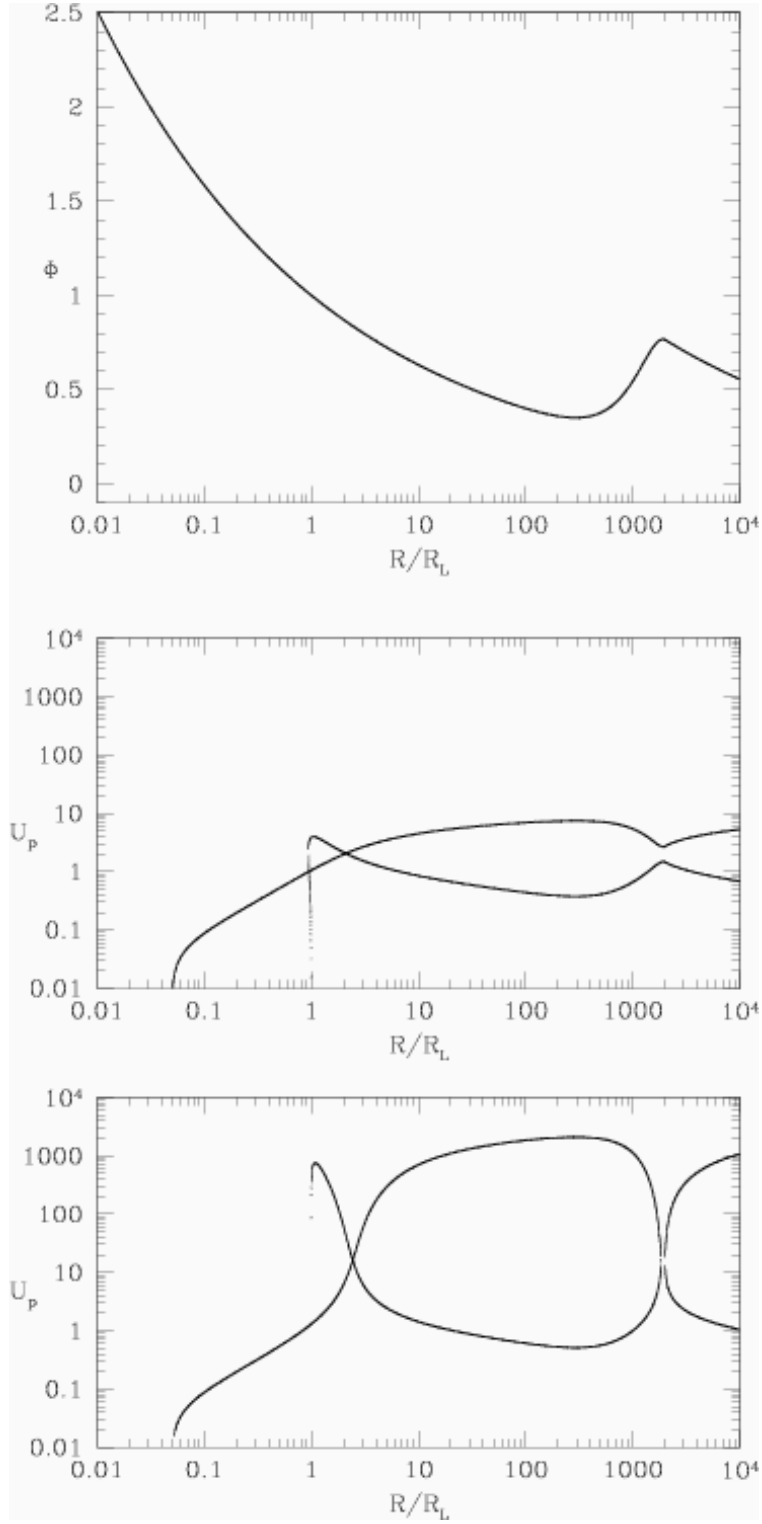


Fig. 6.— Relativistic MHD wind/jet solution. Profiles of the magnetic flux tube function (*top*) and the poloidal velocity (*below*) along the field line for a re-collimating magnetic flux tube. Magnetization $\sigma = 10, 5000$ (from *top* to *bottom*).